# Surface plasmon-waveguide hybrid polymer light-emitting devices using hexagonal Ag dots

**Kwan Hyun Cho,[1] Jin Yeong Kim,[1] Dae-Geun Choi,[2] Ki-Jung Lee,[2] Jun-Hyuk Choi,[2] and Kyung Cheol Choi[1,*]**

[1]*Department of Electrical Engineering, KAIST, Daejeon, Korea*

[2]*Korea Institute of Machinery & Materials, Daejeon, Korea*

**Corresponding author: kyungcc@kaist.ac.kr*

Received October 14, 2011; revised December 7, 2011; accepted December 7, 2011; posted December 7, 2011 (Doc. ID 156432); published February 17, 2012

We investigated surface plasmon-waveguide hybrid resonances for enhancement of light emission in polymer light-emitting diodes (PLEDs). Hybrid waveguide-plasmon resonances in the visible range for waveguide mode and near IR range for surface plasmons were observed by incorporation of hexagonal Ag dot arrays. Considerable overlap between the emission wavelength of the PLEDs and the waveguide mode by an Ag dot array with a lattice constant of 500 nm was observed. Because of enhanced light extraction by Bragg scattering of waveguide modes, photoluminescence (PL) and electroluminescence (EL) were increased by 70% and 50%, respectively. 

*OCIS codes:* 240.6680, 160.5690.

Polymer light-emitting diodes (PLEDs) have been a subject of much interest due to their inexpensive fabrication process and practical applicability to flexible devices. However, improvement of the intrinsic photoluminescence (PL) efficiency and light extraction efficiency of PLEDs remains a critical issue with respect to their commercial application. Light extraction of the indium tin oxide (ITO)/organic waveguide mode of organic and polymer light-emitting diodes (OLEDs/PLEDs) was enhanced by Bragg diffraction using photonic crystal structures [1–3]. Intrinsic PL efficiency of OLEDs/PLEDs was enhanced by excitation of the surface plasmons using randomly arrayed metal nanostructures [4–6]. Periodic metal nanostructures on dielectric waveguides provide a new material class of simultaneous electronic and photonic resonances [7,8]. Metallic photonic crystals provide remarkable optical properties, which include enhancement of light transmission and efficient coupling light from air to waveguide modes, as well as localized surface plasmon (LSP) resonances [7,8].

In this Letter, we investigated waveguide-plasmon hybrid structures that employ a periodic hexagonal Ag dot array for enhancement of light emission in PLEDs. Compared with square structures, hexagonal structures have high degenerate Bragg scattering vectors for light scatterers into waveguide or surface plasmons [9]. Figure 1(a) presents a schematic illustration of the proposed surface plasmon-waveguide hybrid PLED structure. An Ag dot array was fabricated on an ITO with a thickness of 150 nm using nanoimprint lithography and the lift-off process. Ag layers with a thickness of 24 nm were deposited after deposition of a chromium (Cr) adhesion layer with a thickness of 1.5 nm using a thermal evaporation technique. The height of Ag dots must be lower than the thickness of PEDOT:PSS (Poly(3,4-ethylenedioxythiophene): poly (styrenesulfonate)) to prevent an electrical short-circuit. The diameter of the Ag dots was 200 nm, and $D$ denotes the lattice constant of the hexagonal array. The Ag dot array with a lattice constant of 500 nm was observed via scanning electron microscopy (SEM) and atomic force microscopy (AFM), and related images are presented in Figs. 1(c) and (d). PEDOT:PSS with a thickness of 50 nm was spin-coated onto the substrates incorporating the Ag dot arrays, and Poly [2-methoxy-5-(2-ethylhexyloxy)-1,4-phenylenevinhlene] (MEH-PPV) with a thickness of 60 nm was spin-coated onto the samples [10]. LiF (1 nm) and Al (1 nm)/Ag (100 nm) were deposited by thermal evaporation as an electron injection layer and a cathode electrode, respectively.

Absorbance spectra were measured by an ultraviolet-visible (UV-VIS) spectrophotometer (SHIMADZU). The emission spectrum was measured using a LabRAM Raman/PL microscope (HORIBA JOBIN YVON) in reflective mode from the MEH-PPV side. Excitation wavelength of 500 nm using an Xe lamp was employed for emission of MEH-PPV. For the absorbance and PL

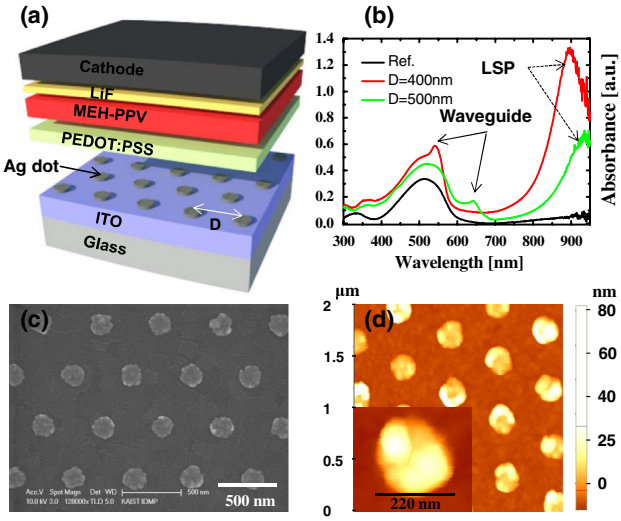


Fig. 1. (Color online) (a) Schematic of the proposed surface plasmon-waveguide hybrid PLED structure. (b) Absorbance spectra of ITO substrate/Ag dots/PEDOT:PSS/MEH-PPV structures. (c) SEM and (d) AFM images of hexagonal Ag dot arrays fabricated on an ITO substrate.

 

measurement, PLED structures without the electron injection layer and the cathode electrode were prepared. The current density-voltage and electroluminescence (EL) intensity-voltage measurements were carried out using a current/voltage source measurement unit (Keithley 2400) and a luminance colorimeter (TOPOCON BM-7A) driven by a Keithley source.

Absorbance spectra of ITO substrate/Ag dot/PEDOT:PSS/MEH-PPV structures with lattice constants of 400 nm and 500 nm are shown in Fig. 1(b). Here, "Ref." denotes the conventional structure without an Ag dot array. Absorbance spectra of the "Ref." sample only present optical absorption of MEH-PPV film with peaks at 510 nm. However, the absorbance spectra of the samples with the Ag dot array show additional resonance peaks of waveguide modes in the visible range and LSPs in the near infrared (IR) range. Compared with the results previously reported by Haynes *et al.* [11], the LSP peak wavelength of 900–950 nm was red-shifted. This is ascribed to the increased refractive index of ITO and polymer compared with air. The LSP resonance at $D = 500$ nm has a longer wavelength than that at $D = 400$ nm due to radiative dipolar coupling [11,12]. In addition, regular arrangement of metal nanostructures on the waveguide, such as an ITO and a polymer layer, can provide efficient coupling from air to waveguide-plasmon polaritons using momentum conservation, as delineated in the following equation: [13,14]:

$$\rightarrow k_{\mathrm{wg}} = \rightarrow k_x \pm m \rightarrow G_x \pm n \rightarrow G_y, \qquad (1)$$

where $\rightarrow k_{\mathrm{wg}}$ is the wave vector of the waveguide mode, $\rightarrow k_x$ is the wave vector of the incident light in the $x$ direction, and $m$ and $n$ are integers. We have the Bragg scattering vectors of $\rightarrow G_x = (4\pi/\sqrt{3}D)[1 \rightarrow x + 0 \rightarrow y]$ and $\rightarrow G_y = (4\pi/\sqrt{3}D)[(1/2) \rightarrow x + (\sqrt{3}/2) \rightarrow y]$ for calculation and measurement associated with the hexagonal array. For normal incident light, $TE_0$ waveguide modes at wavelengths of 540 nm and 642 nm were observed in the samples with $D = 500$ nm and $D = 400$ nm, respectively, which was confirmed on a theoretical basis using a planar waveguide model [15,16]. The wavelength of the MEH-PPV emission in a range from 550 nm to 700 nm was closely related to the waveguide-plasmon polaritons rather than LSP resonance.

To understand the nature of the waveguide-plasmon polaritons, we investigated the absorbance spectra by rotating the samples with a lattice constant of 500 nm. Figure 2(a) shows the absorbance spectra of the $D = 500$ nm sample with incident angles Ω from 0° to 32° by rotating the sample around the $y$ axis with respect to the normal to the surface, as displayed in the inset figure. The six degenerate waveguide modes $[(-1,0), (0,-1), (-1,1), (0,1), (1,-1)$, and $(1,0)]$ are attributed to the Bragg scattering vector by the hexagonal structure. The sets of $(m,n)$ associated with Eq. (1) represent the first order of the scattering event that couples the incident light with a waveguide mode. The positions of the peaks from the absorbance spectra of Fig. 2(a) are shown in Fig. 2(b) with the dispersion relation of energy versus $\rightarrow k_x$. The positions of the absorbance peaks correspond with the theoretically calculated $TE_0$ waveguide

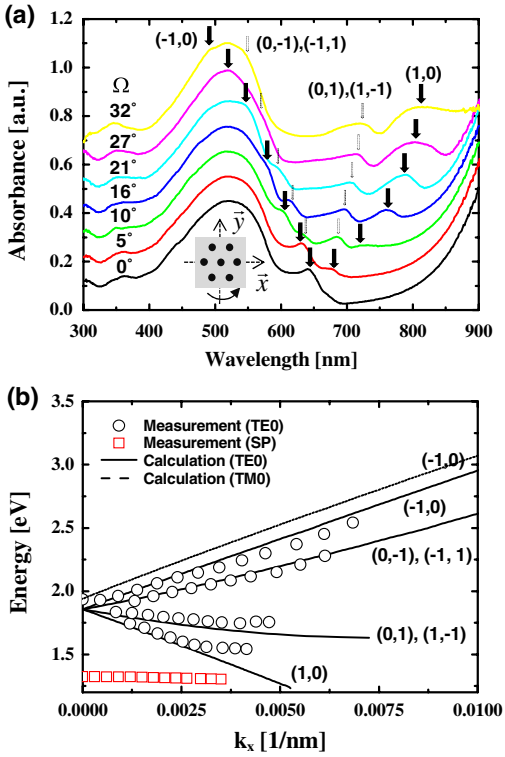


Fig. 2. (Color online) (a) Absorbance spectra for the sample with a lattice constant of 500 nm with incident angles Ω from 0° to 32°. The inset figure shows the geometry of the sample and the measurement scheme. (b) Measured and calculated dispersion relation for the sample with a lattice constant of 500 nm.

mode. However, the waveguide modes [(1,0), (0,1), and (1,1)] are different from the calculation, as $\rightarrow k_x$ is increased. This is attributed to the fact that light is coupled into the polariton due to the LSP resonance at 1.32 eV. Waveguide-plasmon polaritons, quasi-particles formed by the waveguide modes with surface plasmon modes located in their proximity, were observed. The $TM_0$ mode is not distinct due to the weak intensity obtained from the absorbance spectra.

Figure 3 shows the room temperature PL spectra and the PL enhancement ratio for the samples with lattice constants of 400 nm and 500 nm. The highest PL intensity was observed for the sample with $D = 500$ nm at the measurement angle of 0°. This is attributed to the fact that there is considerable overlap between the wavelength of MEH-PPV emission in the range from 550 nm

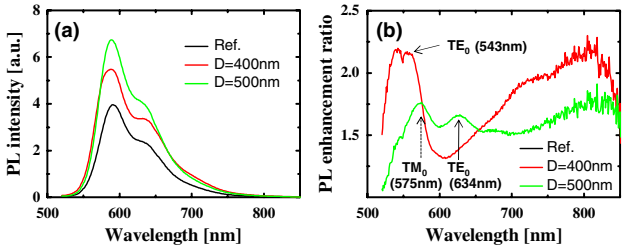


Fig. 3. (Color online) Room temperature PL spectra (a) and PL enhancement ratio (b) for the samples with lattice constants of 400 nm and 500 nm. The PL measurement setup was in the reflective mode from the MEH-PPV side, and the incident angle and measurement angle are 22.5° and 0° (normal).

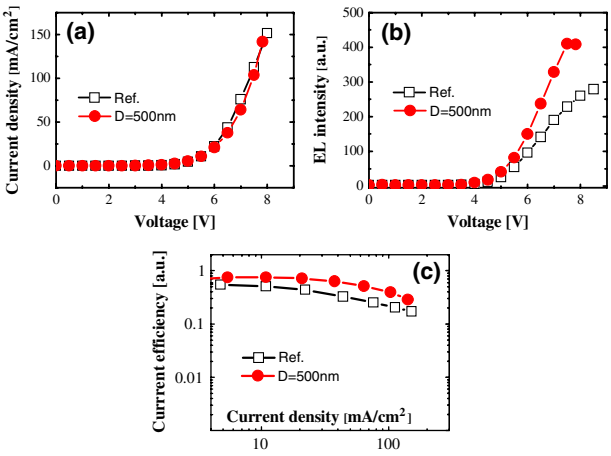


Fig. 4. (Color online) (a) Current density-voltage characteristics (b) and EL intensity-voltage characteristics of PLEDs with and without hexagonal Ag dot array with a lattice constant of 500 nm. (c) Current efficiency as a function of the current density.

to 700 nm and the waveguide-plasmon polaritons with the peak wavelength of 642 nm. The PL enhancement ratio obtained by dividing the spectrum of the structures with and without an Ag dot array shows the wavelength dependence of the enhanced emission. The PL enhancement ratio shows the evidence that the enhanced PL intensity originated from the waveguide-plasmon polaritons by the Ag dot arrays. The peak intensities of the PL enhancement ratio at 543 nm, at 634 nm, and at 575 nm, shown in Fig. 3(b), correspond to the 540 nm (Fig. 1(b)), 642 nm (Fig. 1(b) or Fig. 2), and 637 nm (Fig. 2) for normal incident ($\rightarrow k_x = 0$). The large difference between calculation and measurement of $TM_0$ at normal incident ($\rightarrow k_x = 0$) was due to the photonic energy gap [13], as our calculation used a simple planar waveguide model without a photonic energy gap. Also, PL intensity can be increased using a reflecting mirror or a surface plasmon-photon (SP-photon) coupling due to the roughness of the Ag dot as shown in Fig. 1(d) [17]. However, densities of Ag dot arrays have low values of 14% (at $D = 500$ nm) and 22% (at $D = 400$ nm), respectively. In addition, PL intensity at $D = 500$ nm was more enhanced than that at $D = 400$ nm. Therefore, the enhanced the PL intensity originated from the waveguide-plasmon polaritons due to the Ag dot arrays.

Figures 4(a) and (b) show the current density-voltage and EL intensity-voltage characteristics of PLEDs with and without a hexagonal Ag dot array with a lattice constant of 500 nm, and Fig. 4(c) shows the current efficiency as a function of the current density. EL intensity of the device with the Ag dot array increased relative to the Ref., although the variation of the current density of the devices with the Ag dot array was similar to that of the Ref. As a result, an increase in current efficiency of approximately 50% at a current density of 20 mA/cm$^2$ was observed due to enhanced light extraction by Bragg scattering of waveguide modes.

In summary, hybrid waveguide-plasmon resonances were observed using incorporation of hexagonal Ag dot arrays, which were inserted between an ITO and a polymer layer. Reasonable agreement of the dispersion relation between the theoretical calculation and measurement were obtained. The wavelength of MEH-PPV emission in a range from 550 nm to 700 nm overlapped with the waveguide modes by the Ag dot array with a lattice constant of 500 nm. The waveguide modes, rather than LSP resonances, owing to the Ag dot array with a lattice constant of 400–500 nm, contributed to the light emission of the PLEDs.

This research was supported by the Basic Science Research Program through the National Research Foundation of Korea (NRF) funded by the Ministry of Education, Science and Technology (CAFDC-20100009890), and the Korea Innovation Cluster Foundation (A2010DD005), funded by the Ministry of Knowledge Economy, Korea, in 2010. D.-G. Choi acknowledges support from grant 2009K000069 from the Center for Nanoscale Mechatronics & Manufacturing and grant 10033636 from National Platform Technology.

## References

1. K. Ishihara, M. Fujita, I. Matsubara, T. Asano, S. Noda, H. Ohata, A. Hirasawa, H. Nakada, and N. Shimoji, Appl. Phys. Lett. **90**, 111114 (2007).
2. J. M. Lupton, B. J. Matterson, I. D. Samuel, M. J. Jory, and W. L. Barnes, Appl. Phys. Lett. **77**, 3340 (2000).
3. Y. J. Lee, S. H. Kim, J. Huh, G. H. Kim, Y. H. Lee, S. H. Cho, Y. C. Kim, and Y. R. Do, Appl. Phys. Lett. **82**, 3779 (2003).
4. K. Y. Yang, K. C. Choi, and C. W. Ahn, Appl. Phys. Lett. **94**, 173301 (2009).
5. A. Fujiki, T. Uemura, N. Zettsu, M. Akai-Kasaya, A. Saito, and Y. Kuwahara, Appl. Phys. Lett. **96**, 043307 (2010).
6. H.-J. Park, D. Vak, Y.-Y. Noh, B. Lim, and D.-Y. Kim, Appl. Phys. Lett. **90**, 161107 (2007).
7. A. Christ, S. G. Tikhodeev, N. A. Gippius, J. Kuhl, and H. Giessen, Phys. Rev. Lett. **91**, 183901 (2003).
8. J. Zhang, L. Cai, W. Bai, and G. Song, Opt. Lett. **35**, 3408 (2010).
9. Q. Wang, J. Li, C. Huang, C. Zhang, and Y. Zhu, Appl. Phys. Lett. **87**, 091105 (2005).
10. K. H. Cho, S. I. Ahn, S. M. Lee, C. S. Choi, and K. C. Choi, Appl. Phys. Lett. **97**, 193306 (2010).
11. C. L. Haynes, A. D. McFarland, L. L. Zhao, R. P. Van Duyne, G. C. Schatz, L. Gunnarsson, J. Prikulis, B. Kasemo, and M. Käll, J. Phys. Chem. B **107**, 7337 (2003).
12. W. A. Murray and W. L. Barnes, Adv. Mater. **19**, 3771 (2007).
13. S. Linden, J. Kuhl, and H. Giessen, Phys. Rev. Lett. **86**, 4688 (2001).
14. Q. Wang, J. Li, C. Huang, C. Zhang, and Y. Zhu, Appl. Phys. Lett. **87**, 091105 (2005).
15. C. R. Pollock, *Fundamentals of Optoelectronics* (CBLS, 2003).
16. T. Tamir and R. C. Alferness, *Guided-Wave Optoelectronics* (Springer–Verlag, 1990).
17. K. Okamoto, I. Niki, A. Shvartser, Y. Narukawa, T. Mukai, and A. Scherer, Nat. Mater. **3**, 601 (2004).